Journal of Controlled Release 329 (2021) 353–360

Contents lists available at ScienceDirect

Journal of Controlled Release

journal homepage: www.elsevier.com/locate/jconrel

Antigen folding improves loading efficiency and antitumor efficacy of PC7A nanoparticle vaccine

Jonathan Wilhelm, Manuel Quiñones-Pérez, Jian Wang, Xu Wang, Vijay S. Basava, Jinming Gao *

Department of Pharmacology, Harold C. Simmons Comprehensive Cancer Center, University of Texas Southwestern Medical Center, 6000 Harry Hines Blvd., Dallas, TX 75390, USA

ARTICLE INFO

Keywords:
Ultra-pH sensitive micelles
Peptide encapsulation
Antigen delivery
Cancer vaccine
Secondary structure

ABSTRACT

Cancer vaccines hold great promise to produce antigen-specific T cell immunity for personalized therapy of cancer. Previously, we reported an ultra-pH-sensitive nanoparticle, PC7A, capable of priming an efficacious immune response without significant systemic toxicity. Despite the early success, the relationship between antigen properties and encapsulation efficiency for downstream immune activation remains poorly understood. In this study, we investigated a small library of melanoma antigens and the effects of several formulation methods on the efficiency of peptide loading inside PC7A nanoparticles. Results show loading efficiency is not highly dependent on the formulation methods, but instead mainly driven by the peptide antigen properties. In particular, we identified a phase transition event, namely the folding of antigenic peptides from random coils to α-helical structure, is important for antigen loading inside PC7A nanoparticles. Mutation of a peptide that abrogates the formation of helical structure resulted in poor loading efficiency. Antitumor efficacy studies in melanoma-bearing mice demonstrate the importance of peptide loading in vaccine-induced antitumor immunity. This study highlights the contribution of phase transition of peptide antigens on vaccine formulation in order to make widespread use of personalized nanoparticle vaccines feasible.

1. Introduction

The advent and success of immunotherapy in cancer care spawned a wealth of interest in targeting the immune system to eradicate malignant diseases [1–7]. Immune cells hold the potential to recognize and respond to aberrant protein expressions or mutational burdens by cancer cells, but their response is often compromised by tumor-centric immune suppression [8–11]. Immune checkpoint blockade therapy has improved patient outcomes by inhibiting 'do not kill' signals expressed by the cancer cells to the cytotoxic lymphocytes. However, as life expectancies increase, we are beginning to observe the negative long-term morbidities associated with checkpoint inhibitors, such as autoimmune disorders [12–16]. There is a growing need to improve the tumor specificity of immune therapeutics without causing harm to healthy tissues.

Vaccination therapy for cancer started in the mid-20th century by a set of observations where initial inoculation of tumors was able to generate specific immune responses that reject the re-challenge of the same tumor [17]. With emergence of somatic mutations that provide neoantigen targets for cancer [18–21], the ability to precisely control immune functions against a tumor provides a much more confined immune response over systemic blockade therapies. However, such a personalized approach to immunotherapy makes formulation of therapeutic vaccines a paramount challenge.

Previously, we reported a synthetic ultra-pH-sensitive nanoparticle vaccine, PC7A, which primes efficacious $CD8^+$ T cell responses against a variety of murine tumor models [22,23]. After injection, the PC7A nanoparticle first serves as a delivery vehicle to transport tumor specific antigens through the lymphatic vessels into lymph nodes, where it is endocytosed by antigen presenting cells. During endosomal maturation, organelle acidification leads to the rapid disassembly of the PC7A micelles at a pH of 6.9. Soluble PC7A further disrupts the endosome allowing the PC7A polymer and encapsulated antigen to be released into the cytosol [24]. There, the antigen can be processed via the proteasome for MHC-I presentation, and the PC7A polymer binds and activates stimulator of interferon genes (STING) for type-I interferon production (Fig. 1). Together, these signals provide the necessary cues for robust

* Corresponding author.
E-mail address: jinming.gao@utsouthwestern.edu (J. Gao).

https://doi.org/10.1016/j.jconrel.2020.11.056
Received 7 September 2020; Received in revised form 26 November 2020; Accepted 29 November 2020
Available online 7 December 2020

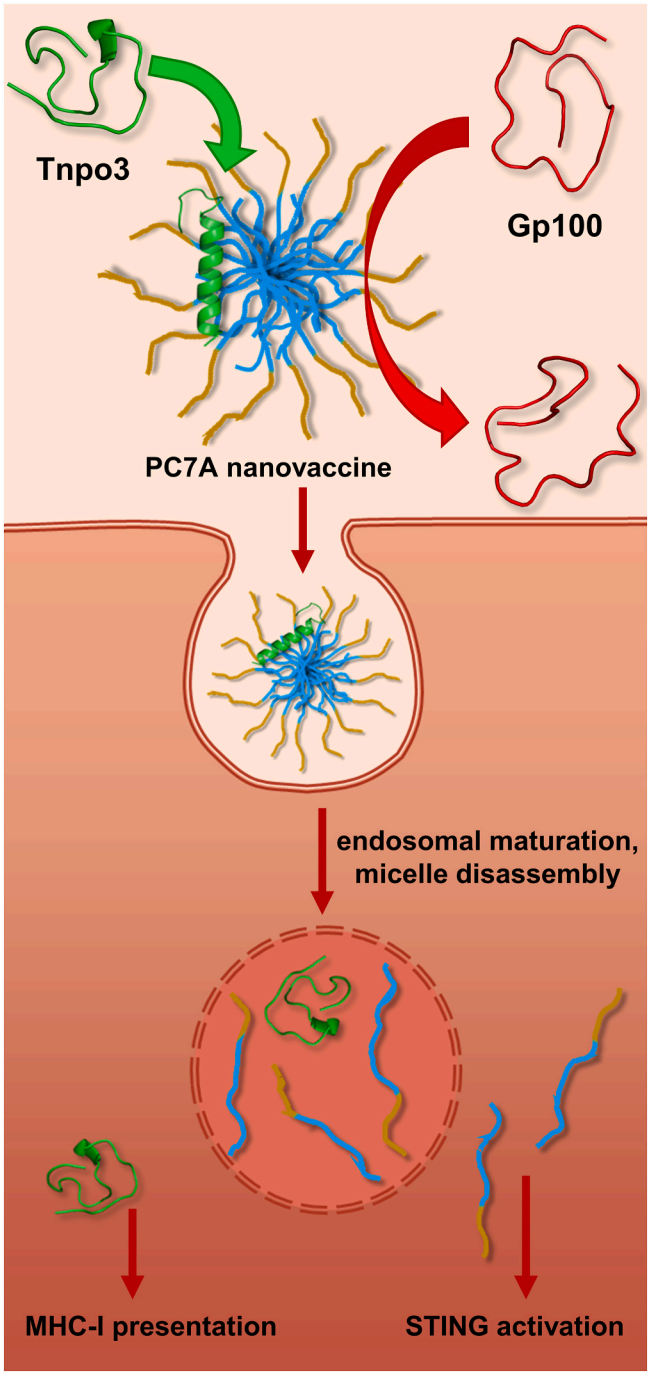

Fig. 1. Certain antigens (like Tnpo3) fold into an α-helix, which drives efficient encapsulation in PC7A micelles for downstream delivery and innate activation to prime a $CD8^+$ T cell response. Antigens without this phase transition event (like Gp100) are poorly loaded and may not be delivered to the targeted immune cells.

$CD8^+$ T cell activation without generating a toxic systemic inflammatory response.

The PC7A nanoparticle serves as a platform technology to produce antigen-specific $CD8^+$ T cell response against tumors. In patient care, this vaccine could be implemented for the delivery of patient-specific tumor antigens following omics analysis and MHC binding prediction from a tumor biopsy [25–28]. However, as a hurdle in the rapid development of personalized cancer vaccines, antigen encapsulation inside PC7A nanoparticles requires careful examination to ensure in vivo antitumor efficacy.

In this study, we investigated the physico-chemical properties of a small library of antigenic peptides which impact their loading efficiency into PC7A micelles. We began with a screen involving tumor associated antigens and neoantigens specific to the B16F10 murine melanoma model. We also evaluated several formulation methods to determine if a specific preparation protocol could be responsible for the boosted encapsulation of antigens. While there was no correlation between bulk amino acid composition and loading efficiency, certain peptides loaded strongly while others did not load, regardless of encapsulation technique. We uncovered that strongly loading peptides fold from a random coil into an α-helix when loaded into the PC7A nanoparticle. An amphipathic alignment of residues along the helix is necessary for this phase transition to occur and provide robust loading for the antigens. These data suggest the importance of secondary structure formation in the design of antigen-loaded nanoparticle vaccines.

2. Materials & methods

2.1. Chemicals

B16F10 melanoma tumor associated antigens $Gp100_{21–41}$ (VGALEGSRNQDWLGVPRQLVT) and $Trp1_{214–237}$ (SHEGPAFLTWHRYHLLQLERDMQE), and neoantigens $Obsl1_{T1764M}$ (REGVELCPGNKYEMRRH GTTHSLVIHD), Pbk_{V145D} (DSGSPFPAAVILRDALHMARGLKYLHQ), $Tnpo3_{G504A}$ (VVDRNPQFLDPVLAYLMKGLCEKPLAS), and mutated antigen Tnpo3LOF (VVDRNPQFLDPVLAYKKKGLCEKPLAS) were synthesized by Biomatik. Amicon Ultra-0.5 and Amicon Ultra-4 centrifugal ultrafiltration devices were purchased from Millipore. Other solvents and reagents were purchased from Fisher Scientific Inc. or Sigma-Aldrich.

2.2. Synthesis and preparation of PC7A micelles

Polyethylene glycol-*b*-poly(2-hexamethyleneimino ethyl methacrylate) (PC7A) was synthesized by atom transfer radical polymerization using previously published procedures [29]. PEG-5 k was used as the initiator and copper chloride and 2,2′-bipyridine were used as the catalyst. 2-(Hexamethyleneimino) ethyl methacrylate (C7A-MA) monomer was synthesized using previously published procedures [30,31]. Micelles were prepared using a solvent evaporation method. Briefly, 10 mg of PC7A polymer was dissolved in 0.5 mL methanol then added into 4 mL milli-Q ultrapure water dropwise under sonication. This mixture was filtered four times to remove methanol using an Amicon Ultra-4 centrifugal ultrafiltration tube (MWCO = 10 k), replenishing the retentate with fresh ultrapure water after each step. After the final filtration, ultrapure water was added to bring the polymer concentration to 10 mg/mL as a stock micelle solution. Following micelle formation, the hydrodynamic diameter (Dh) was measured by dynamic light scattering (DLS, Malvern Nano-ZS Model).

2.3. Antigen loading into PC7A micelles

Individual antigens were each dissolved in ultrapure water to prepare a 1 mg/mL stock solution. Under various loading conditions, detailed in following sub-sections, 150 μL of PC7A micelle stock solution, 25 μL of antigen stock solution, and ultrapure water were mixed to a total volume of 500 μL to evaluate antigen loading at 3 mg/mL PC7A and 50 μg/mL antigen concentrations. The resulting mixture from each technique was allowed to incubate for 30 min at room temperature prior to antigen loading efficiency analysis.

2.3.1. Simple physical mixing

PC7A micelle solution was first diluted in ultrapure water to a concentration of 3 mg/mL. Then, antigen stock solution was added to a concentration of 50 μg/mL and the mixture was rapidly pulse vortexed to mix well.

2.3.2. Basic pH loading condition

PC7A and antigen were mixed according to the protocol in section 2.3.1. While monitoring solution pH, 1.0 M sodium hydroxide solution was added to adjust the solution pH to 10.0. Ultrapure water was added to adjust the final volume to 500 μL.

2.3.3. Acid-base titration

PC7A and antigen were mixed according to the protocol in section 2.3.1. While monitoring solution pH, 1.0 M hydrochloric acid solution was added to adjust the solution pH to 4.0, causing the disassembly of PC7A micelles. Immediately, sodium hydroxide solution was added to adjust the solution pH to 7.4, allowing PC7A micelle self-assembly and subsequent entrapment of antigen. Ultrapure water was added to adjust the final volume to 500 μL.

2.3.4. Salting out method

PC7A and antigen were mixed according to the protocol in section 2.3.1. Then, 75 μL of 1.0 M sodium chloride solution was added and ultrapure water was added to adjust the final volume to 500 μL. The final sodium chloride concentration was 150 mM.

2.3.5. Microfluidic mixing

To force rapid, microvolume mixing of PC7A micelles with antigen, we performed microfluidic mixing at a 1:1 ratio with 6 mg/mL PC7A micelle solution and 100 μg/mL antigen solution using either the fish-bone architecture of NanoAssemblr Chips or an off-the-shelf IDEX PEEK Tee (P-890) [32]. Volumetric flow of each input solution was controlled by a NE-300 syringe pump using HSW 3 mL norm-ject syringes at the maximum possible flow rate (2.76 mL/min).

2.4. Analysis of antigen loading efficiency

After antigen encapsulation in PC7A micelles, the resulting solution was filtered using Amicon Ultra-0.5 (MWCO = 100 k) to separate free soluble antigen from micelle-encapsulated antigen. Ultrafiltration membranes were pretreated with Tween-20 according to a previously published protocol to prevent non-specific adsorption of antigen onto the regenerated cellulose membrane material [33]. Briefly, each ultrafiltration device was incubated with 5% Tween-20 for 5 mins. Then, the Tween-20 was flushed through the membrane by centrifugation at 3000*g* for 10 mins. Residual Tween solution was removed by ultrapure water within the sample chamber of the device.

Following Tween-20 pretreatment, the antigen-loaded micelle solution was loaded into the ultrafiltration device and centrifuged at 3000*g* until 250 μL of solution flowed through to the filtrate. The filtrate was analyzed by high performance liquid chromatography (HPLC) to determine unloaded antigen concentration by comparison to a calibration curve. Loaded antigen was validated by acidifying the retentate to disassemble the micelles for analysis by HPLC. Mass balance calculations were performed to determine the mass of antigen loaded into the PC7A micelles, and loading efficiency (LE) was calculated as follows:

$$LE\ (\%) = \frac{mass\ of\ antigen\ loaded\ inside\ PC7A\ micelles\ (\mu g)}{total\ mass\ of\ antigen\ (\mu g)} \times 100$$

2.5. High performance liquid chromatography (HPLC) analysis

HPLC was performed using an Agilent 1260 Infinity II system equipped with an automatic sampler, quaternary pump, C-18 column, and multi-wavelength detector. A linear gradient of ultrapure water with 0.1% trifluoroacetic acid and HPLC-grade acetonitrile with 0.1% trifluoroacetic acid was used to concentrate each antigen to a specified retention time. Wavelengths 210 nm, 220 nm, and 230 nm were used to measure peptide concentration by absorption in the amine backbone. Wavelengths 254 nm and 280 nm were used to measure peptide concentration for antigens containing aromatic residues. Following peak integration, peak areas were compared to standard curves prepared for each antigen to determine peptide concentration.

2.6. Transmission electron microscopy (TEM) and dynamic light scattering analysis (DLS)

$Tnpo3_{G504A}$-loaded PC7A nanoparticles were prepared according to the protocol in section 2.3.1. Unloaded PC7A nanoparticles were analyzed as a control. Each sample was diluted by a factor of three to achieve a final polymer concentration of 1.0 mg/mL prior to TEM analysis. The solution was placed on a 300-mesh carbon copper grid followed by drying. The grid was then rinsed with distilled water for several seconds to remove any salts before the addition of phosphotungstic acid for negative staining. TEM images were obtained from Tecnai Spirit TEM. For DLS analysis, each sample was diluted by a factor of 100 to achieve a final polymer concentration of 30 μg/mL. Number weighted hydrodynamic diameter (D_h) distributions were recorded using the Malvern Nano-ZS Model (He-Ne Laser, $\lambda = 633$ nm).

2.7. pH-dependent peptide release

$Tnpo3_{G504A}$-loaded PC7A nanoparticles were prepared according to the protocol in section 2.3.1, replacing water with phosphate buffered saline (PBS) at different pH values (7.4 or 6.4). Unloaded antigen was quantified by ultrafiltration followed by HPLC analysis over the course of 4 h. After 4 h, the retentate was acidified to validate the remaining loaded antigen.

2.8. Circular dichroism (CD) spectroscopy

A Jasco J-815 circular dichroism (CD) spectropolarimeter was used to evaluate the secondary structure of antigens (50 μg/mL) before and after mixing with PC7A micelles (500 μg/mL). Spectra were recorded in the far ultraviolet range (180–250 nm). A total of 20 accumulations were averaged together and GraphPad Prism smoothing algorithms (2nd order, 20 neighboring points) were employed to reduce noise caused by nanoparticle light scattering.

2.9. Antigen secondary structure prediction

The secondary structure of each antigen was predicted using the PEP-FOLD 3.5 server made available by the University of Paris Diderot [34]. The server returns 5 predicted structures according to high-quality models for that peptide. We examined each of the models and presented one representative model for each antigen in this article.

2.10. Animals and cells

All animal procedures were performed with ethical compliance and approval by the Institutional Care and Use Committee at the University of Texas Southwestern Medical Center. Female C57BL/6 mice (6–8 weeks) were purchased from Charles River Laboratories. B16-F10 cells were purchased from ATCC. Cells were routinely tested using a mycoplasma contamination kit. Cells were cultured in complete medium (DMEM, 10% fetal bovine serum) at 37 °C in 5% CO_2 and normal O_2.

2.11. Tumor inoculation and treatment

Six to eight week old mice ($n = 8$ per group) were injected subcutaneously with 1.8×10^5 B16-F10 melanoma cells on the right flank. Mice were immunized by subcutaneous injection at the tail base (0.5 μg per antigenic peptide, 30 μg PC7A nanoparticle) on days 5, 10, and 15 after tumor inoculation. Tumor growth was monitored using a digital caliper and tumor size was calculated as 0.5 x length x $width^2$. Mice were sacrificed when tumor size reached 1500 mm^3.

2.12. Dendritic cell and T cell activation by flow cytometry

Healthy 6–8 week old mice (n = 5 per group) were vaccinated subcutaneously (0.5 μg per antigenic peptide, 30 μg PC7A nanoparticle) three times in five day intervals. Twenty four hours after the final vaccination, mice were sacrificed and inguinal lymph nodes were harvested under sterile conditions, and single cell suspensions were prepared. Flow cytometry was performed on a BD LSRFortessa and analyzed using BD FACSDiva 8.0.2 software.

The following primary antibodies were used for staining: aqua fluorescent reactive dye (Invitrogen, Cat# L34966 A), FITC anti-mouse CD3 (Biolegend, Cat# 100203, clone: 17A2), AF700 anti-mouse CD8a (Biolegend, Cat# 100730, clone: 53–6.7), FITC anti-mouse CD11c (Biolegend, Cat# 117306, clone: N418), PerCP anti-mouse CD45 (BD Pharmingen, Cat# 557235, clone: 30-F11), PE anti-mouse CD80 (Biolegend, Cat# 104707, clone: 16-10A1), APC anti-mouse CD86 (Biolegend, Cat# 105012, clone: GL-1), and AF594 anti-mouse/human Ki67 (Biolegend, Cat# 151214, clone: 11F6).

2.13. Statistical analysis

For in vitro loading efficiency analysis, experiments were repeated in triplicate, with error bars representing the standard deviation. Significance between groups was determined by Student's *t*-test. Lack of loading efficiency correlation with antigen primary structure (Table 1) was determined using Pearson's correlation test. For in vivo studies, we used 8 animals/group for tumor treatment studies and 5 animals/group for immunogenicity measurements based on relative pilot studies. Error bars represent standard error of the mean. Statistical significance of tumor growth was determined using two-way ANOVA followed by multiple comparisons. Significance of survival was determined using log-rank test. Significance of immunogenicity was determined using Student's *t*-test. All statistical analysis was performed using GraphPad Prism 8.2.0, and results were considered significant if $P < 0.05$ (*, $P < 0.05$; **, $P < 0.01$; ***, $P < 0.001$).

3. Results

3.1. Antigen loading is divergent depending on peptide

We screened a small library of five peptide antigens for the B16-F10 murine melanoma model (Table 1) for loading into PC7A micelles. The library consists of two tumor associated antigens, $Gp100_{21–41}$ and $Trp1_{214–237}$, and three neoantigens, $Obsl1_{T1764M}$, Pbk_{V145D}, and $Tnpo3_{G504A}$. Antigens were designed as small peptides of 21–27 amino acids spanning the epitope of interest. The screen consisted of six encapsulation techniques, with the goal of elucidating the most effective loading method to employ for all peptides.

The first technique was simple physical mixing, a vortex mixture of antigen and micelles in solution which relies solely on affinity of antigens for the PC7A micelles for encapsulation. Then, we employed a basic condition, with the goal of using a pH of 10.0 to induce a negative charge among the peptides above their isoelectric points (pIs), enhancing attraction to the positively charged surface of PC7A micelles. Next, we used an acid-base titration to force disassembly and reassembly of the PC7A micelles, driving physical entrapment of the antigen. Next, we used sodium chloride as a 'salting out' strategy to reduce the solubility of hydrophobic antigens in solution [35,36] and to enhance hydrophobic interactions between these antigens and the core of PC7A micelles. Finally, we employed two microfluidic mixing platforms, the NanoAssemblr and "off the shelf" IDEX P-890 [32] to force rapid, microvolume mixing of the antigen with the polymer to facilitate the interactions between the two species during micellization.

Results show that antigen loading is not highly dependent on encapsulation methods, but rather on the antigen itself (Fig. 2a), indicating antigen-intrinsic properties are responsible for encapsulation. While some conditions induced higher loading efficiency as in the acid-base titration and the salting out method, there was a much stronger correlation to the individual antigens, with $Tnpo3_{G504A}$ and $Trp1_{214–237}$ exhibiting near complete encapsulation among all techniques, while maintaining particle size and pH-dependent release (Fig. 2b-d). Comparison of antigen encapsulation to physical properties such as peptide composition (hydrophobic, acidic, basic amino acids), charge, size, or isoelectric point (Table 1) did not reveal any correlation via the Pearson correlation test.

3.2. Antigens with efficient encapsulation fold into amphipathic α-helices upon loading

Previous studies have demonstrated the ability of polymeric micelles to serve as a nanocage to convert random coil peptides in solution into α-helices, enabling cell membrane penetration and cytosolic delivery of the peptides [37,38]. To examine the relationship between antigen encapsulation and secondary structure, we began by simulating the secondary structure of each antigen using the PEP-FOLD program [34]. PEP-FOLD predicts secondary structure in physiological solution based on empirical relationships of short sequences derived from observed small protein structures. From the library of antigens, three antigens ($Trp1_{214–237}$, Pbk_{V145D}, and $Tnpo3_{G504A}$) were predicted to have α-helical structure, one antigen ($Obsl1_{T1764M}$) to exhibit β-strand structure, and one antigen ($Gp100_{21–41}$) to maintain random coil morphology (Fig. 3b). The amino acid sequence was mapped onto the predicted secondary structure for each antigen, which revealed an amphipathic alignment of residues along the predicted α-helix for efficient loading $Trp1_{214–237}$ and $Tnpo3_{G504A}$. In contrast, Pbk_{V145D} contains a loop within its predicted α-helix that disrupts amphipathic structure. Therefore, we hypothesized that α-helical structure with amphipathic alignment of residues is responsible for efficient encapsulation in PC7A micelles.

We employed circular dichroism (CD) spectroscopy to investigate the contribution of secondary structure to antigen encapsulation. We modified concentrations to favor cleaner spectra with less noise caused by light scattering from the micelles in solution. CD spectra were recorded in the far UV range (180–250 nm) for all peptides either in pure solution or loaded into PC7A nanoparticles under the simple physical mixture technique. The binary divergence between strongly and weakly loaded antigens (Fig. 2a) yields a clean contrast in secondary structure before and after encapsulation. We found that in pure water, all antigens exhibit a random coil conformation. Upon mixing with PC7A nanoparticles, the spectra of $Tnpo3_{G504A}$ (Fig. 3c) and $Trp1_{214–237}$ shift with

Table 1
Peptide antigens for the B16-F10 murine melanoma model.

Antigen	Sequence	MW (Da)	Charge (pH = 7)	pI	Hydrophobic	Acidic	Basic	Neutral
$Gp100_{21–41}$	VGALEGSRNQDWLGVPRQLVT	2295	−0.2	6.9	7 (33.3%)	2 (9.5%)	2 (9.5%)	10 (47.6%)
$Trp1_{214–237}$	SHEGPAFLTWHRYHLLQLERDMQE	2994	−1.7	5.8	8 (33.3%)	4 (16.7%)	5 (20.8%)	7 (29.2%)
$Obsl1_{T1764M}$	REGVELCPGNKYEMRRHGTTHSLVIHD	3135	0.2	7.3	7 (25.9%)	4 (14.8%)	7 (25.9%)	9 (33.3%)
Pbk_{V145D}	DSGSPFPAAVILRDALHMARGLKYLHQ	2964	1.2	9.8	9 (33.3%)	2 (7.4%)	5 (18.5%)	11 (40.7%)
$Tnpo3_{G504A}$	VVDRNPQFLDPVLAYLMKGLCEKPLAS	3017	−0.1	6.3	11 (40.7%)	3 (11.1%)	3 (11.1%)	10 (37.0%)

We employed this small library of antigens to study the relationship between encapsulation efficiency and antigen properties.

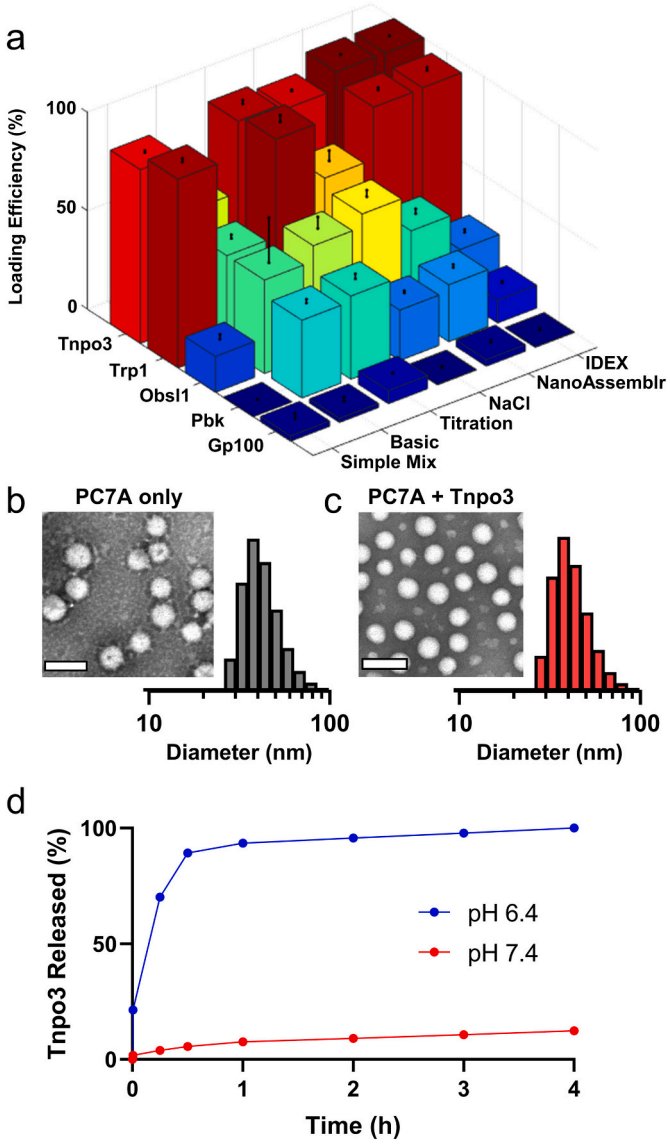

Fig. 2. Screen of antigenic peptides and loading methods on loading efficiency of melanoma antigens. (a) Loading screen reveals peptide loading efficiency is mainly dependent on antigens but not on loading technique. (b, c) TEM (image, scale bar 100 nm) and DLS (number weighted hydrodynamic diameter distributions) measurements reveal size and morphology of PC7A nanoparticles remains similar before (b) and after (c) loading with a representative antigen, $Tnpo3_{G504A}$. (d) Antigen loading of representative $Tnpo3_{G504A}$ is relatively stable above the transition pH of PC7A. When pH falls below the transition point to a pH of 6.4, Tnpo3 is rapidly released from the micelles.

emerging maxima around 190 nm and shoulder peak formation around 220 nm. CD spectra of typical α-helical proteins contain negative bands at 222 and 208 nm, and a positive band at 193 nm [39]. This result confirms the predicted folding and formation of α-helical structures in $Tnpo3_{G504A}$ and $Trp1_{214–237}$. In contrast, $Gp100_{21–41}$ (Fig. 3d), $Obsl1_{T1764M}$, and Pbk_{V145D} (Fig. 3e) maintain as random coils even after mixing with PC7A micelles. Despite its predicted α-helical structure, Pbk_{V145D} lacks the α-helical folding seen with $Tnpo3_{G504A}$ and $Trp1_{214–237}$. The predicted and experimental structure discrepancy in Pbk_{V145D} indicates that an empirical propensity to form helical structures is not sufficient for encapsulation, and supports the need for amphipathic alignment of residues along the helix for efficient loading in PC7A micelles.

3.3. Amphipathic α-helix is necessary for efficient encapsulation in PC7A micelles

To further examine the apparent dependence of encapsulation on secondary structure-amphipathic alignment, we synthesized a loss of function $Tnpo3_{G504A}$ peptide with disrupted alignment, referred to as $Tnpo3_{LOF}$. The loss of function mutation was introduced by transitioning adjacent leucine and methionine residues to two lysine residues (Fig. 4a). We found that using the simple physical mixing technique, the loss of function mutation led to a significant decrease in loading efficiency of the Tnpo3 peptide (Fig. 4b). Although predictive modeling still suggested an α-helical structure for the $Tnpo3_{LOF}$ peptide, circular dichroism spectroscopy revealed that $Tnpo3_{LOF}$ maintains a random coil conformation before and after mixing with PC7A nanoparticles (Fig. 4c). Together, these data suggest that amphipathic alignment of the $Tnpo3_{G504A}$ peptide and phase transition into the α-helical state on mixing with PC7A micelles are necessary for strong encapsulation into the nanoparticle.

3.4. Efficient peptide loading is necessary to prime an efficacious immune response

To evaluate the effect of peptide loading on antitumor efficacy, we treated C57Bl/6 mice bearing the B16F10 melanoma model with a vaccine formulation under varying conditions. The complete vaccine formulation employed for this experiment includes the two antigens with efficient encapsulation, $Tnpo3_{G504A}$ and $Trp1_{214–237}$ (0.5 μg each), mixed with PC7A nanoparticles (30 μg) in phosphate buffered saline (PBS) at a pH of 7.4. Under this condition, the antigens are loaded into the nanoparticles for robust delivery. To deliver PC7A nanoparticles and antigens in the absence of antigen folding (and associated encapsulation), we vaccinated mice with physically separated solutions of PC7A on the right flank and peptide solution on the left flank. Finally, to maintain the presence of both PC7A and antigen components within a single injection but without antigen encapsulation in the micelle state, we prepared the vaccine in PBS at a pH of 6.4 to disassemble the PC7A micelles.

Results show that the vaccine formulation at pH 7.4 was able to achieve an efficacious anti-tumor immune response which prolonged the survival of treated mice through activation of dendritic cells which led to proliferation of cytotoxic T cells (Fig. 5). The physical separation of peptide and nanoparticle demonstrated moderate efficacy. By disassembling the PC7A micelle and preventing antigen encapsulation using pH 6.4, the tumor growth rate and animal survival resemble the antigen alone or PBS alone control groups, indicating abrogation of antitumor efficacy.

4. Discussion

Elucidation of interactions between peptide antigens and polymeric micelles is important to achieve the desired immunological response for nanoparticle vaccines. Previous studies showed peptides and regions of proteins that associate with membrane surfaces exhibit an amphipathic α-helical structure, with a hydrophobic region exposed to the membrane and a hydrophilic region exposed to the surrounding aqueous environment [40–42]. The core-shell interface of the PEG-*b*-PC7A micelles resembles that of a membrane-solution interface, with a hydrophobic PC7A core and a hydrophilic PEG shell. In this study, we took a biophysical approach to investigate peptide folding on antigen loading in the PC7A nanoparticle vaccine. Divergent loading efficiency among a small library of antigens offered molecular insights on the biophysical drivers of encapsulation. Lack of correlation with amino acid composition clarified that loading efficiency is not driven by simple attractive interactions. In silico model prediction suggested a correlation between α-helical secondary structure and high loading efficiency in PC7A micelles. Circular dichroism spectroscopy revealed that efficiently loaded

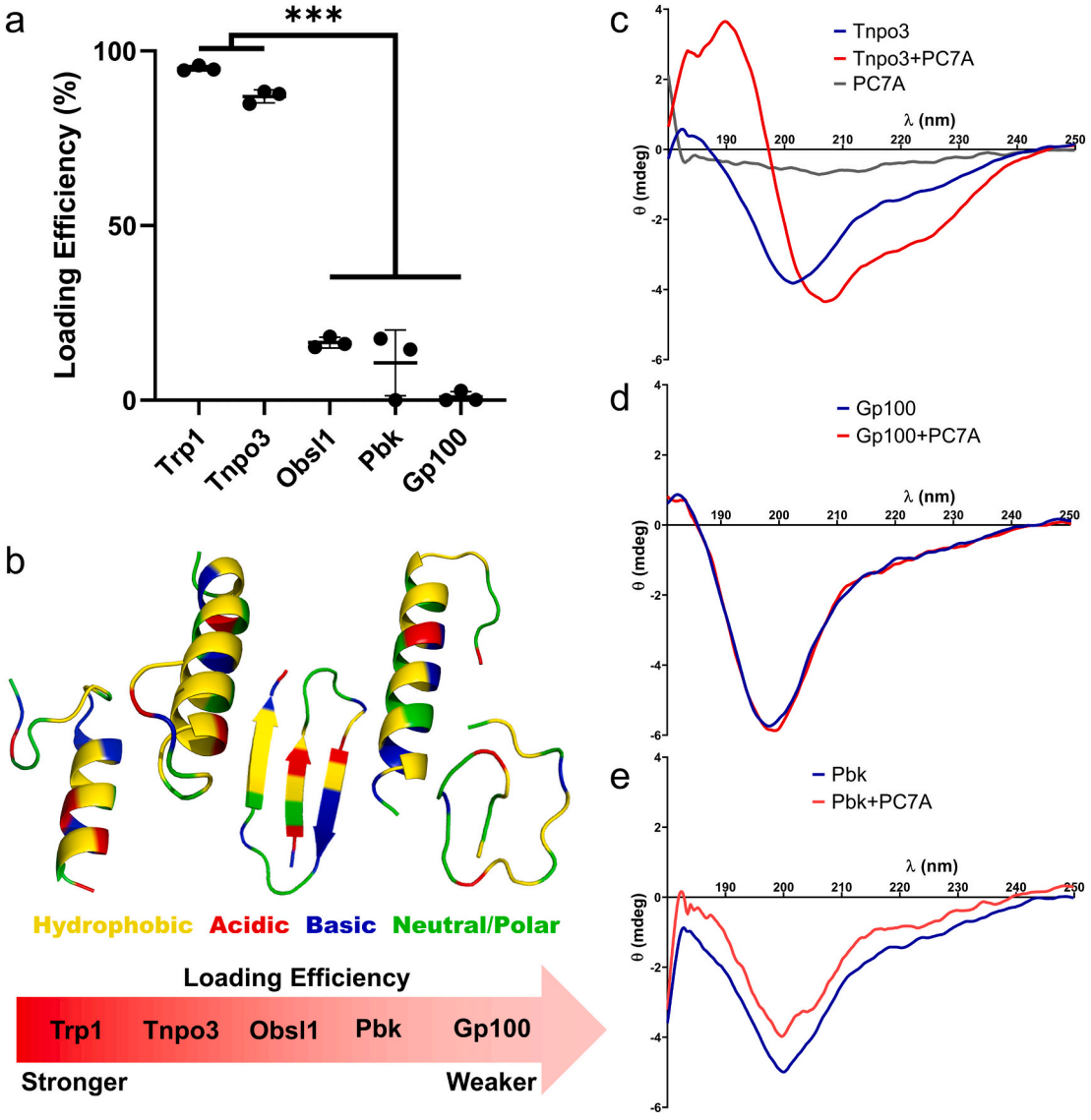

Fig. 3. Secondary structure prediction and circular dichroism spectroscopy reveal peptide folding impacts loading efficiency. (a, b) The predicted secondary structure for each antigen correlates with loading efficiency by simple physical mixing, with higher loading antigens exhibiting amphipathic α-helical structure. (c) Strongly loading antigens, like $Tnpo3_{G504A}$, form α-helical structures upon mixing with PC7A micelles. (d) Poorly loading antigens, like $Gp100_{21–41}$, maintain random coil morphology before and after mixing with PC7A micelles. (e) Despite predicted α-helical structure, Pbk_{V145D} maintains random coil morphology even after mixing, likely due to its lack of amphipathic alignment of residues. Data are presented as means ± s.d. Statistical significance was calculated by Student's *t*-test: ***$P < 0.001$.

peptides folded from a random coil into an α-helix structure upon interaction with the PC7A nanoparticles.

Prediction of α-helical structure alone is insufficient to support efficient encapsulation of antigen into PC7A micelles. Rather, amphipathic alignment of amino acid residues along the predicted helix also appears necessary for antigen folding and associated encapsulation, which may be further stabilized via hydrophobic interactions between hydrophobic amino acids and tertiary amines in the micelle core. In the case of Pbk_{V145D}, an aspartic acid residue disrupts the amphipathic alignment of the predicted helix. This lack of alignment prevents antigen folding and encapsulation. Synthetic disruption of amphipathic alignment in $Tnpo3_{G504A}$ by charged lysine residues has an identical effect as that seen in Pbk_{V145D}.

The insight of a phase transition event for efficient peptide loading suggests the incorporation of similar designs to improve the encapsulation of poorly loaded antigens. Without the efficient loading of antigens, the anti-tumor immune function of the PC7A nanovaccine is compromised. We propose that an amphipathic helical 'anchor' sequence could be amended to each of the poorly loaded antigens, allowing their folding and encapsulation in PC7A micelles for downstream immune function. Molecular engineering of antigen structures may be necessary to the success of nanoparticle vaccines as platform technologies when targeting novel neoantigen sequences for personalized immunotherapy of cancer.

Credit author contribution statement

Jonathan Wilhelm: Conceptualization, Methodology, Validation, Formal analysis, Investigation, Writing – Original Draft, Visualization. **Manuel Quiñones-Pérez**: Methodology, Investigation, Data Curation. **Jian Wang**: Investigation, Resources. **Xu Wang**: Investigation, Resources. **Vijay S Basava**: Investigation. **Jinming Gao**: Conceptualization, Writing – Review & Editing, Supervision, Project administration, Funding acquisition.

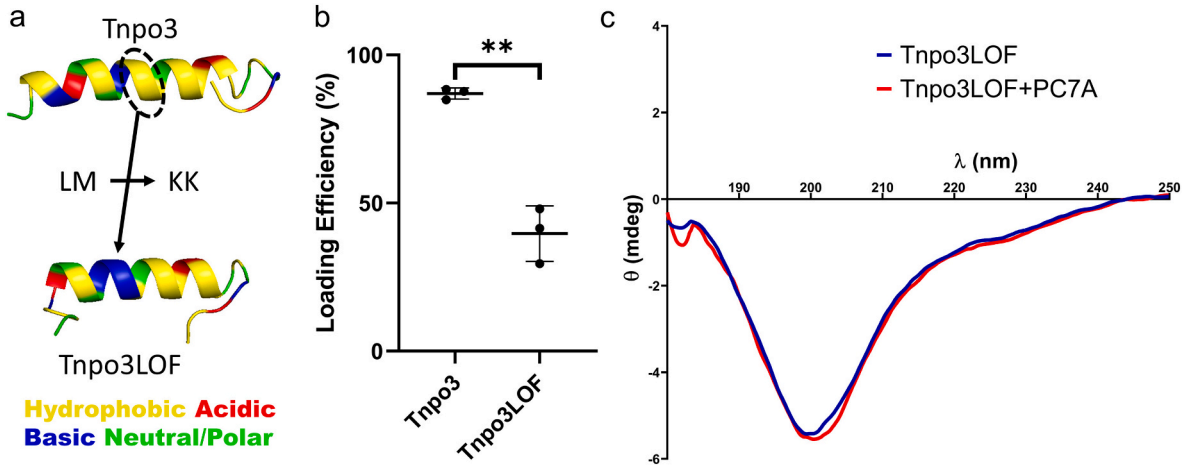

Fig. 4. Disruption of amphipathic alignment of residues along the α-helix of $Tnpo3_{G504A}$ disturbs loading efficiency and helix folding in the PC7A nanoparticle. (a) A loss of function mutation to $Tnpo3_{G504A}$ was introduced by transitioning a leucine and methionine residue to two lysine residues. (b) The loss of function peptide exhibited significantly lower loading efficiency than the native peptide. (c) Circular dichroism spectroscopy reveals that $Tnpo3_{LOF}$ maintains random coil structure after mixing with PC7A, unlike the native $Tnpo3_{G504A}$ peptide which folds into an α-helix on loading into PC7A nanoparticles. Data are presented as means ± s.d. Statistical significance was calculated by Student's *t*-test: $^{**}P < 0.01$.

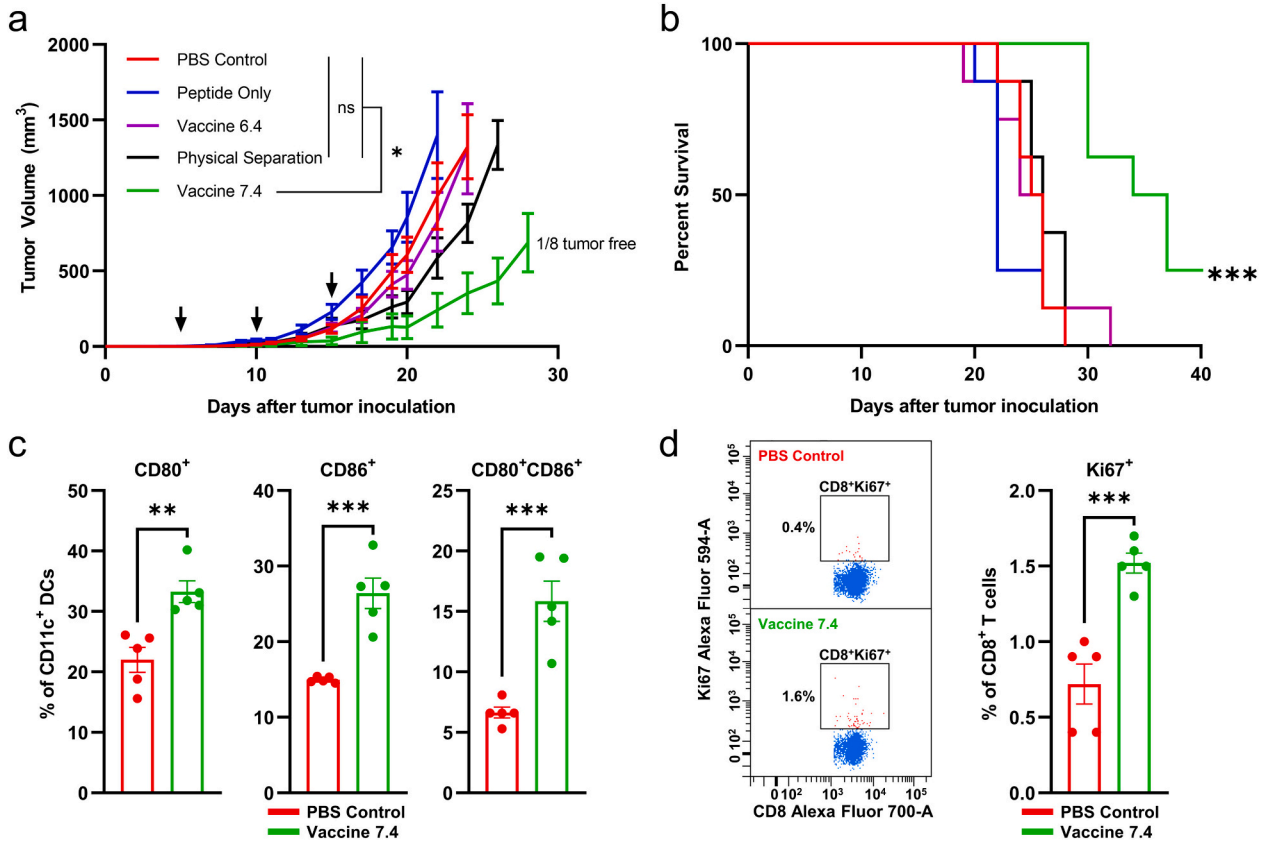

Fig. 5. Efficient antigen loading in the PC7A nanoparticles is necessary for anti-tumor response. (a, b) While the complete vaccine formulation including efficient loading antigens $Tnpo3_{G504A}$ and $Trp1_{214–237}$ primes a robust anti-tumor immune response against B16F10 melanoma, the disruption of antigen folding and encapsulation prevents the downstream immune activation and associated tumor control. Mice were treated on days 5, 10, and 15 with the indicated regimens ($n = 8$ per group). Tumor growth data (a) are shown as mean ± s.e.m. with statistical significance calculated by two-way ANOVA with multiple comparisons: $^{*}P < 0.05$. Kaplan-Meier survival curves (b) are shown with statistical significance calculated by the log-rank test: $^{***}P < 0.001$. (c, d) Healthy mice ($n = 5$ per group) were treated subcutaneously with the vaccine pH 7.4 formulation or PBS three times in five-day intervals. After 24 h post final injection, inguinal lymph nodes were removed for flow cytometry analysis. The complete vaccine formulation at pH 7.4 achieved robust immune response through the activation of dendritic cells (c) which led to the proliferation of $CD8^+$ T cells (d). Representative flow dot plots are shown. Summarized flow data represent mean ± s.e.m. with statistical significance calculated by Student's *t*-test: $^{**}P < 0.01$, $^{***}P < 0.001$.

Declaration of Competing Interest

Jinming Gao is a founder and scientific advisor of OncoNano Medicine, Inc. No other authors have any competing interests.

Acknowledgements

This work was supported by the National Institutes of Health (R01CA216839 and U01CA218422) and Mendelson-Young Endowment in Cancer Therapeutics. We thank Dr. Chad Brautigam and Dr. Shih-Chia Tso of the UT Southwestern Macromolecular Biophysics Resource for assistance with circular dichroism experiments.

References

[1] D.R. Leach, M.F. Krummel, J.P. Allison, Enhancement of antitumor immunity by CTLA-4 blockade, Science 271 (1996) 1734.
[2] F.S. Hodi, S.J. O'Day, D.F. McDermott, R.W. Weber, J.A. Sosman, J.B. Haanen, R. Gonzalez, C. Robert, D. Schadendorf, J.C. Hassel, W. Akerley, A.J. van den Eertwegh, J. Lutzky, P. Lorigan, J.M. Vaubel, G.P. Linette, D. Hogg, C. H. Ottensmeier, C. Lebbé, C. Peschel, I. Quirt, J.I. Clark, J.D. Wolchok, J.S. Weber, J. Tian, M.J. Yellin, G.M. Nichol, A. Hoos, W.J. Urba, Improved survival with ipilimumab in patients with metastatic melanoma, N. Engl. J. Med. 363 (2010) 711–723.
[3] D.M. Pardoll, The blockade of immune checkpoints in cancer immunotherapy, Nat. Rev. Cancer 12 (2012) 252–264.
[4] C. Robert, G.V. Long, B. Brady, C. Dutriaux, M. Maio, L. Mortier, J.C. Hassel, P. Rutkowski, C. McNeil, E. Kalinka-Warzocha, K.J. Savage, M.M. Hernberg, C. Lebbé, J. Charles, C. Mihalcioiu, V. Chiarion-Sileni, C. Mauch, F. Cognetti, A. Arance, H. Schmidt, D. Schadendorf, H. Gogas, L. Lundgren-Eriksson, C. Horak, B. Sharkey, I.M. Waxman, V. Atkinson, P.A. Ascierto, Nivolumab in previously untreated melanoma without BRAF mutation, N. Engl. J. Med. 372 (2014) 320–330.
[5] C. Robert, A. Ribas, J.D. Wolchok, F.S. Hodi, O. Hamid, R. Kefford, J.S. Weber, A. M. Joshua, W.-J. Hwu, T.C. Gangadhar, A. Patnaik, R. Dronca, H. Zarour, R. W. Joseph, P. Boasberg, B. Chmielowski, C. Mateus, M.A. Postow, K. Gergich, J. Elassaiss-Schaap, X.N. Li, R. Iannone, S.W. Ebbinghaus, S.P. Kang, A. Daud, Anti-programmed-death-receptor-1 treatment with pembrolizumab in ipilimumab-refractory advanced melanoma: a randomised dose-comparison cohort of a phase 1 trial, Lancet 384 (2014) 1109–1117.
[6] P. Sharma, J.P. Allison, The future of immune checkpoint therapy, Science 348 (2015) 56–61.
[7] S.M. Ansell, A.M. Lesokhin, I. Borrello, A. Halwani, E.C. Scott, M. Gutierrez, S. J. Schuster, M.M. Millenson, D. Cattry, G.J. Freeman, S.J. Rodig, B. Chapuy, A. H. Ligon, L. Zhu, J.F. Grosso, S.Y. Kim, J.M. Timmerman, M.A. Shipp, P. Armand, PD-1 blockade with nivolumab in relapsed or refractory Hodgkin's lymphoma, N. Engl. J. Med. 372 (2015) 311–319.
[8] H. Dong, S.E. Strome, D.R. Salomao, H. Tamura, F. Hirano, D.B. Flies, P.C. Roche, J. Lu, G. Zhu, K. Tamada, V.A. Lennon, E. Celis, L. Chen, Tumor-associated B7-H1 promotes T-cell apoptosis: a potential mechanism of immune evasion, Nat. Med. 8 (2002) 793–800.
[9] C. Blank, I. Brown, A.C. Peterson, M. Spiotto, Y. Iwai, T. Honjo, T.F. Gajewski, PD-L1/B7H-1 inhibits the effector phase of tumor rejection by T Cell Receptor (TCR) transgenic CD8⁺ T cells, Cancer Res. 64 (2004) 1140.
[10] D.F. Quail, J.A. Joyce, Microenvironmental regulation of tumor progression and metastasis, Nat. Med. 19 (2013) 1423–1437.
[11] P. Sharma, S. Hu-Lieskovan, J.A. Wargo, A. Ribas, Primary, adaptive, and acquired resistance to cancer immunotherapy, Cell 168 (2017) 707–723.
[12] G.Q. Phan, J.C. Yang, R.M. Sherry, P. Hwu, S.L. Topalian, D.J. Schwartzentruber, N.P. Restifo, L.R. Haworth, C.A. Seipp, L.J. Freezer, K.E. Morton, S.A. Mavroukakis, P.H. Duray, S.M. Steinberg, J.P. Allison, T.A. Davis, S.A. Rosenberg, Cancer regression and autoimmunity induced by cytotoxic T lymphocyte-associated antigen 4 blockade in patients with metastatic melanoma, Proc. Natl. Acad. Sci. 100 (2003) 8372.
[13] A. Ribas, L.H. Camacho, G. Lopez-Berestein, D. Pavlov, C.A. Bulanhagui, R. Millham, B. Comin-Anduix, J.M. Reuben, E. Seja, C.A. Parker, A. Sharma, J. A. Glaspy, J. Gomez-Navarro, Antitumor activity in melanoma and anti-self responses in a phase I trial with the anti-cytotoxic T lymphocyte-associated antigen 4 monoclonal antibody CP-675,206, J. Clin. Oncol. 23 (2005) 8968–8977.
[14] K.E. Beck, J.A. Blansfield, K.Q. Tran, A.L. Feldman, M.S. Hughes, R.E. Royal, U. S. Kammula, S.L. Topalian, R.M. Sherry, D. Kleiner, M. Quezado, I. Lowy, M. Yellin, S.A. Rosenberg, J.C. Yang, Enterocolitis in patients with cancer after antibody blockade of cytotoxic T-lymphocyte-associated antigen 4, J. Clin. Oncol. 24 (2006) 2283–2289.
[15] N. Abdel-Wahab, M. Shah, M.E. Suarez-Almazor, Adverse events associated with immune checkpoint blockade in patients with cancer: A systematic review of case reports, PLoS One 11 (2016).
[16] L. Hofmann, A. Forschner, C. Loquai, S.M. Goldinger, L. Zimmer, S. Ugurel, M. I. Schmidgen, R. Gutzmer, J.S. Utikal, D. Göppner, J.C. Hassel, F. Meier, J. K. Tietze, I. Thomas, C. Weishaupt, M. Leverkus, R. Wahl, U. Dietrich, C. Garbe, M. C. Kirchberger, T. Eigentler, C. Berking, A. Gesierich, A.M. Krackhardt, D. Schadendorf, G. Schuler, R. Dummer, L.M. Heinzerling, Cutaneous, gastrointestinal, hepatic, endocrine, and renal side-effects of anti-PD-1 therapy, Eur. J. Cancer 60 (2016) 190–209.
[17] L.J. Old, E.A. Boyse, Immunology of experimental tumors, Annu. Rev. Med. 15 (1964) 167–186.
[18] S.D. Brown, R.L. Warren, E.A. Gibb, S.D. Martin, J.J. Spinelli, B.H. Nelson, R. A. Holt, Neo-antigens predicted by tumor genome meta-analysis correlate with increased patient survival, Genome Res. 24 (2014) 743–750.
[19] M.S. Rooney, S.A. Shukla, C.J. Wu, G. Getz, N. Hacohen, Molecular and genetic properties of tumors associated with local immune cytolytic activity, Cell 160 (2015) 48–61.
[20] T.N. Schumacher, R.D. Schreiber, Neoantigens in cancer immunotherapy, Science 348 (2015) 69.
[21] V. Thorsson, et al., The immune landscape of cancer, Immunity 48 (2018) 812–830 (e814).
[22] M. Luo, H. Wang, Z. Wang, H. Cai, Z. Lu, Y. Li, M. Du, G. Huang, C. Wang, X. Chen, M.R. Porembka, J. Lea, A.E. Frankel, Y.-X. Fu, Z.J. Chen, J. Gao, A STING-activating nanovaccine for cancer immunotherapy, Nat. Nanotechnol. 12 (2017) 648–654.
[23] M. Luo, Z. Liu, X. Zhang, C. Han, L.Z. Samandi, C. Dong, B.D. Sumer, J. Lea, Y.-X. Fu, J. Gao, Synergistic STING activation by PC7A nanovaccine and ionizing radiation improves cancer immunotherapy, J. Control. Release 300 (2019) 154–160.
[24] Z. Wang, M. Luo, C. Mao, Q. Wei, T. Zhao, Y. Li, G. Huang, J. Gao, A redox-Activatable fluorescent sensor for the high-throughput quantification of cytosolic delivery of macromolecules, Angew. Chem. Int. Ed. Eng. 56 (2017) 1319–1323.
[25] M.M. Van Buuren, J.J.A. Calis, T.N.M. Schumacher, High sensitivity of cancer exome-based CD8 T cell neo-antigen identification, OncoImmunology 3 (2014).
[26] M.M. Gubin, M.N. Artyomov, E.R. Mardis, R.D. Schreiber, Tumor neoantigens: building a framework for personalized cancer immunotherapy, J. Clin. Investig. 125 (2015) 3413–3421.
[27] X.S. Liu, E.R. Mardis, Applications of Immunogenomics to Cancer, Cell 168 (2017) 600–612.
[28] T.J. O'Donnell, A. Rubinsteyn, M. Bonsack, A.B. Riemer, U. Laserson, J. Hammerbacher, MHCflurry: open-source class I MHC binding affinity prediction, Cell Syst. 7 (2018) 129–132 (e124).
[29] N.V. Tsarevsky, K. Matyjaszewski, "Green" atom transfer radical polymerization: from process design to preparation of well-defined environmentally friendly polymeric materials, Chem. Rev. 107 (2007) 2270–2299.
[30] K. Zhou, Y. Wang, X. Huang, K. Luby-Phelps, B.D. Sumer, J. Gao, Tunable, ultrasensitive pH-responsive nanoparticles targeting specific endocytic organelles in living cells, Angew. Chem. Int. Ed. 50 (2011) 6109–6114.
[31] K. Zhou, H. Liu, S. Zhang, X. Huang, Y. Wang, G. Huang, B.D. Sumer, J. Gao, Multicolored pH-tunable and activatable fluorescence nanoplatform responsive to physiologic pH stimuli, J. Am. Chem. Soc. 134 (2012) 7803–7811.
[32] E. Bottaro, C. Nastruzzi, "Off-the-shelf" microfluidic devices for the production of liposomes for drug delivery, Mater. Sci. Eng. C 64 (2016) 29–33.
[33] K.-J. Lee, R. Mower, T. Hollenbeck, J. Castelo, N. Johnson, P. Gordon, P.J. Sinko, K. Holme, Y.-H. Lee, Modulation of nonspecific binding in ultrafiltration protein binding studies, Pharm. Res. 20 (2003) 1015–1021.
[34] Y. Shen, J. Maupetit, P. Derreumaux, P. Tufféry, Improved PEP-FOLD approach for peptide and miniprotein structure prediction, J. Chem. Theory Comput. 10 (2014) 4745–4758.
[35] W. Melander, C. Horváth, Salt effects on hydrophobic interactions in precipitation and chromatography of proteins: an interpretation of the lyotropic series, Arch. Biochem. Biophys. 183 (1977) 200–215.
[36] R.L. Baldwin, How Hofmeister ion interactions affect protein stability, Biophys. J. 71 (1996) 2056–2063.
[37] X. Fang, T. Yang, L. Wang, J. Yu, X. Wei, Y. Zhou, C. Wang, W. Liang, Nano-cage-mediated refolding of insulin by PEG-PE micelle, Biomaterials 77 (2016) 139–148.
[38] Z. Liu, C. Zhou, Y. Qin, Z. Wang, L. Wang, X. Wei, Y. Zhou, Q. Li, H. Zhou, W. Wang, Y.-X. Fu, M. Zhu, W. Liang, Coordinating antigen cytosolic delivery and danger signaling to program potent cross-priming by micelle-based nanovaccine, Cell Discov. 3 (2017) 17007.
[39] S.M. Kelly, T.J. Jess, N.C. Price, How to study proteins by circular dichroism, Biochim. Biophys. Acta (BBA) Proteins Proteomics 1751 (2005) 119–139.
[40] D. Eisenberg, R.M. Weiss, T.C. Terwilliger, The helical hydrophobic moment: a measure of the amphiphilicity of a helix, Nature 299 (1982) 371–374.
[41] W.S. Davidson, A. Jonas, D.F. Clayton, J.M. George, Stabilization of α-Synuclein secondary structure upon binding to synthetic membranes, J. Biol. Chem. 273 (1998) 9443–9449.
[42] Y. Shai, Mechanism of the binding, insertion and destabilization of phospholipid bilayer membranes by α-helical antimicrobial and cell non-selective membrane-lytic peptides, Biochim. Biophys. Acta Biomembr. 1462 (1999) 55–70.